

Parameter fine-tuning method for MMG model using real-scale ship data

Rin Suyama^{a,*}, Rintaro Matsushita^b, Ryo Kakuta^b, Kouki Wakita^a and Atsuo Maki^{a,*}

^aDepartment of Naval Architecture and Ocean Engineering, Graduate School of Engineering, Osaka University, 2-1 Yamadaoka, Suita, Osaka 565-0971, Japan

^bMonohakobi Technology Institute Co., Ltd., Yusen Building, 3-2 Marunouchi, 2-Chome, Chiyoda-ku, Tokyo 100-0005, Japan

ARTICLE INFO

Keywords:

Autonomous Vessel
System Identification
Fine-Tuning
Real-scale Ship Data
CMA-ES

ABSTRACT

In this paper, a fine-tuning method of the parameters in the MMG model for the real-scale ship is proposed. In the proposed method, all of the arbitrarily indicated target parameters of the MMG model are tuned simultaneously in the framework of SI using time series data of real-scale ship maneuvering motion data to steadily improve the accuracy of the MMG model. Parameter tuning is formulated as a minimization problem of the deviation of the maneuvering motion simulated with given parameters and the real-scale ship trials, and the global solution is explored using CMA-ES. By constraining the exploration ranges to the neighborhood of the previously determined parameter values, the proposed method limits the output in a realistic range. The proposed method is applied to the tuning of 12 parameters for a container ship with five different widths of the exploration range. The results show that, in all cases, the accuracy of the maneuvering simulation is improved by applying the tuned parameters to the MMG model, and the validity of the proposed parameter fine-tuning method is confirmed.

1. Introduction

The development of maneuvering models is essential to the research and the development of autonomous navigation algorithms. Autonomous navigation algorithms, studied intensively by institutions in many countries in recent years, should be validated by maneuvering simulators. The reliability of the algorithm can be improved by testing it under maneuvering simulators with accurate maneuvering models.

Research on modern maneuvering models has a long history, with literature dating back to the 1940s, such as Davidson and Schiff (1946). The maneuvering models have been studied in terms of hydrodynamics by Motora (1959); Inoue et al. (1981) and control engineering by Motora (1955); Nomoto et al. (1957). In addition, researches have been conducted on models of the hydrodynamic forces of individual components, such as hull, propeller, and rudder. For instance, Abkowitz (1964); Åström and Källström (1976) utilized Taylor expansion with respect to state variables to derive a maneuvering model. The MMG model (Ogawa and Kasai, 1978; Yasukawa and Yoshimura, 2015) was groundbreaking in that it could represent each individual component and their interaction. Fossen (2011) formulated a maneuvering model in vector form inspired by mechanical systems, and this formulation is often used in model-based control design. In addition, there exist studies on models expressed with polynomials of motion states and actuator states (Miyachi et al., 2023; Dong et al., 2023). In contrast to these white box models, some studies have addressed the

approximation of maneuvering models using black box models based on machine learning. Some examples of the black box models are artificial neural networks (ANN) (Moreira and Soares, 2003; Rajesh and Bhattacharyya, 2008; Zhang and Zou, 2013; Oskin et al., 2013; Luo and Zhang, 2016; Woo et al., 2018; He et al., 2022; Wakita et al., 2022; Wang et al., 2023), support vector machine (Luo and Zou, 2009; Wang et al., 2020), and Gaussian process (Ramirez et al., 2018; Xue et al., 2020).

Among various maneuvering models, the MMG model has high accuracy in simulations of maneuvering motion. This is explained by the fact that it is formulated based on detailed hydrodynamics. Due to its high performance, the MMG model is widely used for the design and validation of autonomous navigation algorithms. Li et al. (2013) validated the path following control law based on sliding mode control by numerical simulations following the MMG model. Zhang et al. (2017) validated the course keeping control law with nonlinear feedback in a simulation based on the MMG model. Zheng et al. (2022) designed a path following control of an unmanned surface vessel by applying the framework of reinforcement learning with the state transition model based on the MMG model. There are also examples of simulations based on the MMG model that solve the autonomous berthing/unberthing problems in the framework of off-line trajectory planning (Maki et al., 2020; Miyachi et al., 2022b; Suyama et al., 2022).

The MMG model contains constant parameters to be identified. There have been various methods for the identification of parameters in the MMG model for model-scale ships. Classically, captive tests were conducted to identify the parameters (Ogawa and Kasai, 1978; Yasukawa and Yoshimura, 2015). Computational fluid dynamics (CFD) is also used for the identification of the parameters in the MMG

*Corresponding author

Email addresses: suyama_rin@naoe.eng.osaka-u.ac.jp (R. Suyama); rintaro_matsushita@monohakobi.com (R. Matsushita); ryo_kakuta@monohakobi.com (R. Kakuta); kouki_wakita@naoe.eng.osaka-u.ac.jp (K. Wakita); maki@naoe.eng.osaka-u.ac.jp (A. Maki)

ORCID(s):

model (Zhang et al., 2019). Sakamoto et al. (2019) identified the values of the parameters in the MMG model based on the captive model tests simulated with CFD.

So far in most cases, the parameters for the real-scale ship MMG model were identified based on the results of model-scale captive tests. One of the differences between the maneuvering motion of model-scale ships and real-scale ships is the difference in Reynolds numbers. To correct the effect of the difference in Reynolds numbers, for instance, for limited parameters such as the frictional resistance coefficient for an equivalent flat plate and the wake coefficient in straight moving, there are widely used methods such as the three-dimensional extrapolation method (e.g. (Yasukawa and Yoshimura, 2015)).

However, at this time, the methodology for the identification of the parameters in the real-scale ship MMG model using captive tests is not established. Some parameters, such as the flow straightening coefficient, are sometimes used without correcting for the effect of the difference in Reynolds numbers, although the effects have been noted (Aoki et al., 2006). In addition, the effects of the difference in Reynolds numbers are not completely clarified for all parameters in the MMG model. If captive tests on real-scale ships were conducted, the parameters could be identified without being affected by the difference in Reynolds numbers, but captive tests on large ships, such as containers, are not possible.

Another method for identification of the parameters in the real-scale ship MMG model is a heuristic tuning of previously determined values by referring to the maneuvering motion data of the real-scale ship. In most cases, this tuning is implemented by experienced engineers using their own heuristic methods based on their senses (Sutulo and Soares, 2014). This heuristic tuning directly refers to real-scale ship maneuvering motion data, so the accuracy of the MMG model with the tuned parameters can be steadily improved. However, heuristic tuning of a large number of parameters is not optimal, so an automatic tuning method needs to be established.

System identification (SI) is applicable for the determination of the values of parameters in the real-scale ship MMG model. SI is an identification framework for system parameters using input/output data of the target system. Therefore, SI for the parameters in the MMG model of real-scale ships can be implemented only with time series data of the maneuvering motion of the subject real-scale ship. SI has been applied to parameter identification of ship maneuvering models. Kalman filter is one of the popular methods for SI, and Åström and Källström (1976); Abkowitz (1980) applied Kalman filter to the Abkowitz model. A combination of state estimation and SI was proposed by (Yoon and Rhee, 2003) for parameter identification. Araki et al. (2012) validated the SI method using the maneuvering motion data simulated using CFD. Sutulo and Soares (2014) adopted the genetic algorithm as the exploration method for the optimal values of parameters in SI. This study was extended to SI for the maneuvering model with a modular structure (Sutulo and Soares, 2023). Miyauchi et al. (2022a)

proposed a parameter identification method for the MMG model without the initial guess of the parameters using the SI framework. This study was extended to the parameter identification of the Abkowitz model with more than 200 parameters and validated its effectiveness (Miyauchi et al., 2023). However, in the method proposed by Miyauchi et al. (2022a, 2023), maneuvering motion data with random inputs, which is difficult to obtain in the operation of real-scale ships, were used, and the validation of the method was limited to model-scale ship cases. Several studies on SI utilize time series data of real-scale ship maneuvering motion (Abkowitz, 1980; Kim, 2018; Meng et al., 2022; Kambara et al., 2022; Wang et al., 2023), but these studies have focused on certain components of the maneuvering model, linear maneuvering models, or ANN models. To the best of the authors' knowledge, the SI method for the whole MMG model using real-scale ship data is not discussed.

In this study, the authors propose a fine-tuning method for all of the arbitrarily indicated target parameters of the MMG model using the framework of SI. The proposed method is designed to automatically fine-tune the parameter values previously determined based on hydrodynamics, captive model tests, and CFD to the ones for the real-scale MMG model. The proposed method directly refers to the time series data of real-scale ship maneuvering motion and steadily improves the performance of the MMG model with the tuned parameter in terms of the accuracy of the simulated maneuvering motion. The parameter tuning is formulated as a constrained minimization problem, and the solution is explored using Covariance Matrix Adaption Evolutionary Computation (CMA-ES) (Hansen, 2007; Hansen and Auger, 2014). To obtain realistic values for the MMG parameters, the ranges of available values for the target parameters in the fine-tuning problem are constrained to the neighborhood of the previously determined values. The proposed parameter fine-tuning method is applied to a container ship with $L_{pp} = 83\text{m}$ and validated. The objective of this study is not to clarify the effect of the difference in Reynolds numbers between real-scale ships and model-scale ships, but to establish a practical method for fine-tuning MMG parameters.

The rest of the manuscript is organized as follows. Sec.2 describes the notation used in this manuscript. The MMG model of the subject ship of this study is detailed in Sec.3. The proposed parameter fine-tuning method is described in Sec.4. Sec.5 details the CMA-ES. Sec.6 shows the results of parameter tuning for a container ship. The discussion on the proposed method is presented in Sec.7. Sec.8 concludes this manuscript.

2. Notation

\mathbb{R} represents the set of all real numbers. $|x|$ represents the absolute value of $x \in \mathbb{R}$. The overdot “ $\dot{\cdot}$ ” represents the derivative with respect to time t . A^T represents the transposed array of the array A .

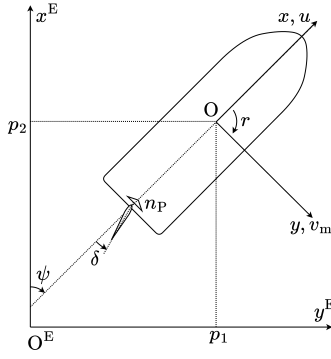

Fig. 1: Coordinate systems.

Table 1

Principal particulars of the subject ship.

Item	Value
L_{pp} [m]	83.0
B [m]	13.5
d [m]	3.8
C_b	0.737
x_G [m]	0.93
D_p [m]	2.80
H_R [m]	3.49
A_R [m ²]	6.282

3. MMG model

First, coordinate systems are defined as Fig. 1 shows. $O - xy$ in Fig. 1 represents a body-fixed coordinate system with the origin fixed at the midship. The ship is assumed to move on an Earth-fixed coordinate system $O^E - x^E y^E$. In this study, the subject ship was a container ship *M. V. SUZAKU*. The principal particulars of the subject ship are summarized in Tab. 1. The maneuvering motion of the ship is represented with state variables:

$$p(t) := (p_1(t) \ p_2(t) \ \psi(t))^T, \quad (1)$$

$$\xi(t) := (u(t) \ v_m(t) \ r(t))^T. \quad (2)$$

The augmented variable:

$$\zeta(t) := (p(t)^T \ \xi(t)^T)^T \in \mathbb{R}^6 \quad (3)$$

is defined. The control input is defined as

$$\tau(t) := (n_p(t) \ \delta(t))^T. \quad (4)$$

The physical meaning of each component of these variables is summarized in Tab. 2. Each component of these variables follows the coordinate systems in Fig. 1. In this study, the authors only consider forward motion with forward propeller revolution; $u(t) > 0$ and $n_p(t) > 0$. In addition, current and wind are ignored as they are assumed to have little effect on the maneuvering motion in this study. In the following,

Table 2

Explanation of symbols.

Vector	Elements	Description
p	p_1	Position on the Earth-fixed frame.
	p_2	Position on the Earth-fixed frame.
	ψ	Heading angle.
ξ	u	Surge velocity.
	v_m	Sway velocity at the midship.
	r	Yaw angular velocity.
τ	n_p	Propeller revolution number.
	δ	Rudder angle.

(t), which indicates the dependence of variables on time, is omitted to simplify the description.

States p and ξ follow the kinematics equation:

$$\dot{p} = R(p)\xi, \quad (5)$$

where

$$R(p) := \begin{pmatrix} \cos \psi & -\sin \psi & 0 \\ \sin \psi & \cos \psi & 0 \\ 0 & 0 & 1 \end{pmatrix}. \quad (6)$$

The equation of motion of ship maneuvering is formulated as

$$\begin{cases} (m + m_x)\dot{u} - (m + m_y)v_m r - x_G m r^2 = X \\ (m + m_y)\dot{v}_m + (m + m_x)ur + x_G m \dot{r} = Y \\ (I_g + x_G^2 m + J_{zz})\dot{r} + x_G m(\dot{v}_m + ur) = N \end{cases} \quad (7)$$

where m , m_x , m_y , I_g , J_{zz} , x_G are the displacement, the added mass for surge motion, the added mass for sway motion, the moment of inertia for yaw motion along the vertical line passing the midship, the added moment of inertia for yaw motion, x coordinate of the center of gravity of the ship, respectively. X , Y , and N in Eq. (7) represent the forces and moments, excluding centrifugal forces, on the body fixed coordinate system $O - xy$. The MMG model (Yasukawa and Yoshimura, 2015) represents X , Y , and N as the sum of the effects of the hull force, propeller force, and rudder force as follows:

$$\begin{cases} X(\theta^t) = X_H + X_P + X_R \\ Y(\theta^t) = Y_H + Y_P + Y_R \\ N(\theta^t) = N_H + N_P + N_R \end{cases} \quad (8)$$

where the argument θ^t represents the target parameter to be tuned. The target parameter θ^t is detailed in Sec.4.1. The MMG model's representation of hull force, propeller force, and rudder force is unique in that it even takes into account the interference and interaction of each component, as detailed below. By reshaping Eq. (7), the system for ξ is obtained as

$$\dot{\xi} = f_{\text{MMG}}(\xi, \tau; \theta^t), \quad (9)$$

where

$$f_{\text{MMG}}(\xi, \tau; \theta^t) := M^{-1} \begin{pmatrix} X(\theta^t) + (m + m_y)v_m r + x_G m r^2 \\ Y(\theta^t) - (m + m_x)ur \\ N(\theta^t) - x_G m r^2 \end{pmatrix}, \quad (10)$$

$$M := \begin{pmatrix} m + m_x & 0 & 0 \\ 0 & m + m_y & x_G m \\ 0 & x_G m & I_g + x_G^2 m + J_{zz} \end{pmatrix}. \quad (11)$$

Augmenting Eq. (5) and Eq. (9), the system for ζ is obtained as

$$\dot{\zeta} = f_\zeta(\zeta, \tau; \theta^t), \quad (12)$$

where

$$f_\zeta(\zeta, \tau; \theta^t) := \left((R(p)\xi)^\top (f_{\text{MMG}}(\xi, \tau; \theta^t))^\top \right)^\top. \quad (13)$$

The following sections detail the hydrodynamic force model for each component. The MMG model used in this study is based on the one proposed by Okuda et al. (2023). However, the model for hull force was the widely used polynomial model.

In this manuscript, characters with the prime symbol represent nondimensionalized quantities. The nondimensionalized values of physical quantities with unit [m], [kg], [kgm²], and [m/s] are calculated by dividing with L_{pp} , $0.5\rho L_{\text{pp}}^2 d$, $0.5\rho L_{\text{pp}}^4 d$, and U , respectively, where $U := \sqrt{u^2 + v_m^2}$ is the ship speed. In the following, $\beta := \arctan(-v_m/u)$ represents the drift angle.

3.1. Hull force (Okuda et al., 2023)

The surge force, the sway force, and the yaw moment induced by the interaction between the ship hull and the fluid were modeled as follows:

$$\begin{cases} X_H = \frac{1}{2}\rho L_{\text{pp}} d U^2 X'_H(v'_m, r') \\ Y_H = \frac{1}{2}\rho L_{\text{pp}} d U^2 Y'_H(v'_m, r') \\ N_H = \frac{1}{2}\rho L_{\text{pp}}^2 d U^2 N'_H(v'_m, r') \end{cases} \quad (14)$$

The nondimensionalized forces and moment were modeled as

$$\begin{cases} X'_H(v'_m, r') = -R'_0 + X'_{vv} v_m'^2 + X'_{vr} v'_m r' + X'_{rr} r'^2 \\ \quad + X'_{vvv} v_m'^3 + X'_{vvv} v_m'^4 \\ Y'_H(v'_m, r') = Y'_v v'_m + Y'_r r' \\ \quad + Y'_{vv} v_m'^3 + Y'_{vvr} v_m'^2 r' \\ \quad + Y'_{vrr} v_m' r'^2 + Y'_{rrr} r'^3 \\ N'_H(v'_m, r') = N'_v v'_m + N'_r r' \\ \quad + N'_{vvv} v_m'^3 + N'_{vvr} v_m'^2 r' \\ \quad + N'_{vrr} v_m' r'^2 + N'_{rrr} r'^3 \end{cases} \quad (15)$$

where the coefficients are constant parameters which are called the hydrodynamic derivatives.

3.2. Propeller force (Okuda et al., 2023)

The propeller force for $u > 0$ and $n_p > 0$ was modeled as

$$\begin{cases} X_P = \frac{1}{2}\rho S_P V_r^2 (1 - t_p) K_T(\phi_P) \\ Y_P = \frac{1}{2}\rho S_P V_r^2 C_{PY}(\phi_P) \\ N_P = \frac{1}{2}\rho S_P L_{\text{pp}} V_r^2 C_{PN}(\phi_P) \end{cases}. \quad (16)$$

Here t_p is a constant parameter called the thrust deduction factor. ϕ_P is defined as

$$\phi_P := \frac{180}{\pi} \arctan\left(\frac{u_p}{0.7\pi n_p D_P}\right) \quad (17)$$

where $u_p := (1 - w_p)u$. The function $K_T(\phi_P)$ was modeled as

$$K_T(\phi_P) = 3.31 \times 10^{-6} \phi_P^3 - 3.72 \times 10^{-4} \phi_P^2 - 2.60 \times 10^{-3} \phi_P + 0.167, \quad (18)$$

by fitting measured data in the propeller open test shown in Fig.6 in the original paper (Okuda et al., 2023). The function $C_{PY}(\phi_P)$, $C_{PN}(\phi_P)$ were modeled as

$$C_{PY}(\phi_P) = -2.83 \times 10^{-5} \phi_P^2 + 6.04 \times 10^{-4} \phi_P - 1.28 \times 10^{-2}, \quad (19)$$

$$C_{PN}(\phi_P) = \begin{cases} -2.48 \times 10^{-4} \phi_P - 1.70 \times 10^{-3} & \text{for } \phi_P < 20, \\ -1.86 \times 10^{-4} \phi_P + 4.03 \times 10^{-3} & \text{for } \phi_P \geq 20, \end{cases} \quad (20)$$

by fitting measured data shown in Fig.13 in the original paper (Okuda et al., 2023). In addition,

$$S_P := \frac{\pi D_P^2}{4} \quad (21)$$

is the propeller disk area, and

$$V_r := \sqrt{u_p^2 + (0.7\pi n_p D_P)^2} \quad (22)$$

is the apparent inflow velocity into the propeller. Here the wake fraction factor w_p was modeled as

$$w_p = w_{p0} \exp(C_w \beta_p^2) \quad (23)$$

where

$$\beta_p := \beta - l'_p r' \quad (24)$$

is the geometrical inflow angle of the propeller with $l'_p = -0.5$, w_{p0} is the value of w_p at $\beta_p = 0$.

3.3. Rudder force (Okuda et al., 2023)

The surge force, sway force, and yaw moment induced by the rudder were modeled as follows:

$$\begin{cases} X_R = -(1 - t_R)F_N \sin \delta \\ Y_R = -(1 + a_H)F_N \cos \delta \\ N_R = -(x_R + a_H x_H)F_N \cos \delta \end{cases} \quad (25)$$

The rudder normal force F_N was model as

$$F_N = \frac{1}{2} \rho A_R U_R^2 \{f_\alpha(\delta_f) \sin \alpha_R + C_{10}(\delta_f)\} \quad (26)$$

where A_R is the rudder area,

$$U_R := \sqrt{u_R^2 + v_R^2} \quad (27)$$

is the resultant inflow velocity of the rudder, and

$$\alpha_R := \delta - \text{atan2}(v_R, u_R) \quad (28)$$

is the effective inflow angle of the rudder. The longitudinal inflow velocity component of the rudder u_R was modeled as

$$u_R = \max\{u_R^*, u_R^{**}\} \quad (29)$$

where

$$\begin{cases} u_R^* = u_P \epsilon \left\{ \eta_R \kappa \left(\sqrt{1 + \frac{8K_T(\phi_P)}{\pi J_P^2}} - 1 \right) + 1 \right\}, \\ u_R^{**} = 0.7 \pi n_P D_P u_{R0}. \end{cases} \quad (30)$$

Here, ϵ is the ratio of the wake fraction factors at the propeller and rudder positions, κ is an experimental constant, and

$$\eta_R := \frac{D_P}{H_R} \quad (31)$$

is the ratio of the diameter of the propeller to the rudder height. The lateral inflow velocity component of the rudder v_R was modeled as

$$v_R = \gamma_R (U \sin \beta - l_R r) \quad (32)$$

where l_R is an experimental constant, and γ_R is a constant determined based on

$$\gamma_R = \begin{cases} \gamma_{Rp} & \text{for } \beta_R > 0 \\ \gamma_{Rn} & \text{for } \beta_R < 0 \end{cases} \quad (33)$$

with effective inflow angle

$$\beta_R := \beta - l'_R r' \quad (34)$$

$f_\alpha(\cdot)$ and $C_{10}(\cdot)$ in Eq. (26) was modeled as functions of the flap angle δ_f with

$$f_\alpha(\delta_f) = f_{\alpha 0} + f_{\alpha 2} \delta_f^2 \quad (35)$$

$$C_{10}(\delta_f) = C_{101} \delta_f + C_{103} \delta_f^3 \quad (36)$$

where $f_{\alpha 0}$, $f_{\alpha 2}$, C_{101} , and C_{103} are constants.

The flap angle δ_f is determined depending upon the rudder angle δ in the manipulation system of the subject ship. The relationship between δ and δ_f is shown in Fig.5 in the original paper (Okuda et al., 2023).

Table 3

Pre-determined values of the added masses and added moment of inertia (Okuda et al., 2023).

Item	Value
m'_x	0.010
m'_y	0.168
J'_{zz}	0.010

Table 4

Pre-determined values of the parameters in the model of X_H , Y_H , and N_H (Okuda et al., 2023).

Item	Value	Item	Value	Item	Value
R'_0	0.017	Y'_v	-0.329	N'_v	-0.106
X'_{vv}	0.009	$Y'_r - m'_x$	0.090	N'_r	-0.057
$X'_{vr} + m'_y$	0.160	Y'_{vvv}	-0.787	N'_{vvv}	-0.037
X'_{rr}	-0.0164	Y'_{vvr}	-0.022	N'_{vvr}	-0.105
X'_{vvvr}	-0.824	Y'_{vrr}	-0.206	N'_{vrr}	0.012
X'_{vvvv}	-0.114	Y'_{rrr}	0.001	N'_{rrr}	-0.008

Table 5

Pre-determined values of the parameters in the model of X_P , Y_P , and N_P (Okuda et al., 2023).

Item	Value
t_P	0.080
w_{p0}	0.422
C_w	-2.0

Table 6

Pre-determined values of the parameters in the model of X_R , Y_R , and N_R (Okuda et al., 2023).

Item	Value	Item	Value
t_R	-0.058	γ_{Rp}	0.483
a_H	0.158	γ_{Rn}	0.172
x'_H	-0.605	$f_{\alpha 0}$	2.411
ϵ	1.27	$f_{\alpha 2}$	-0.381
κ	0.5	C_{101}	1.164
u_{R0}	0.14	C_{103}	-0.381
l'_R	-0.888		

3.4. Pre-determined parameter values

The parameters included in the MMG model described in the previous sections have values determined based on hydrodynamics, captive model tests, and CFD, without using the time series of real-scale ship trials. In this manuscript, these values are referred to as *pre-determined* values. The pre-determined values of the parameters used in this study are those given in the original paper (Okuda et al., 2023).

The pre-determined values of added masses and added moment of inertia are shown in Tab. 3. Moreover, the pre-determined values of the parameters used in the models of hydrodynamic forces and moments are shown in Tabs. 4 to 6.

4. Parameter tuning method

In this section, the target parameter to be tuned, the exploration range for the target parameter, the real-scale ship trials used in this study, and the mathematical formulation of the parameter tuning problem are described.

4.1. Target parameter

In this study, among the parameters included in the MMG model shown in Sec.3, the following 12 parameters were set as the target parameter θ^t to be tuned.

$$\theta^t := (R'_0 t_P w_{P0} C_w t_R a_H x'_H \epsilon \kappa l'_R \gamma_{Rp} \gamma_{Rn})^T \quad (37)$$

The target parameters were limited to the ones that have a big influence on the simulated forces and moment. However, the hydrodynamic derivatives were excluded from the target for the simplification of the problem. On the other hand, R'_0 was included in the target of the tuning without applying the extrapolation method. The objective for this is to obtain an average value of R'_0 concerning the variation of ship speed due to maneuvering motion.

The applicability of the proposed method is not limited to the case with the target parameter Eq. (37). The target parameter can be selected arbitrarily by the users.

4.2. Exploration range

In the parameter tuning, the exploration ranges for all elements of θ^t were limited. In this study, it is assumed that all of the parameters in the MMG model of the model-scale ship of the subject ship have their values which have been determined based on hydrodynamics, captive model tests, and CFD. The exploration ranges were set to be the neighborhood of those values. By constraining the ranges of available values for the target parameters in the fine-tuning problem to the neighborhood of the pre-determined values, the proposed method limits the output in realistic ranges.

In the following, the candidate value and the pre-determined value of the target parameter $\theta^t \in \mathbb{R}^{12}$ are described as $\hat{\theta} \in \mathbb{R}^{12}$ and $\theta^{\text{pre}} \in \mathbb{R}^{12}$, respectively. The exploration range for the element of $\hat{\theta}_i$ ($i = 1, \dots, 12$) was formulated as

$$\hat{\Theta}_i := [\theta_i^{\text{pre}} - a_r |\theta_i^{\text{pre}}|, \theta_i^{\text{pre}} + a_r |\theta_i^{\text{pre}}|] \quad (38)$$

with $a_r > 0$. The present study considered the hydrodynamics underlying the maneuvering motion to some extent by defining the exploration range with reference to the pre-determined values. Further investigation of the exploration range for parameters based on the theoretical background is one of the issues for future research. The exploration range of $\theta^t \in \mathbb{R}^{12}$ is described as

$$\hat{\Theta} := \prod_{i=1}^{12} \hat{\Theta}_i . \quad (39)$$

Five cases of parameter fine-tuning with $a_r = 0.2, 0.3, 0.4, 0.5, 0.6$ were conducted for the subject ship.

4.3. Real-scale ship trials data

In this study, the time series of real-scale ship trials were utilized. One time series was treated as matrix $D \in \mathbb{R}^{8 \times T}$ with

$$(D_{1i} \dots D_{8i})^T := (p^i \xi^i \tau^i)^T, \quad (40)$$

$$i = 1, \dots, T .$$

T is the number of time steps included in the time series data with the time step size: $\Delta t = 1.0$ s. Elements p^i , ξ^i , and τ^i represent p , ξ , and τ at the time step i , respectively. In this study, eight turning tests of the subject ship with $\delta = \pm 10, \pm 20, \pm 35, \pm 40$ deg. were prepared and are described as $D^{\pm 10}, D^{\pm 20}, D^{\pm 35}, D^{\pm 40}$, respectively. Fig. 2 exemplifies $D^{\pm 10}$.

These time series data were utilized both for the parameter tuning and the test of the tuned parameter. In the parameter tuning phase, the parameter that minimizes the deviation between numerically simulated time series and the real-scale ship data was explored. In the test phase, the tuned parameter was applied to the simulation of real-scale ship data which was not utilized in the tuning phase and evaluated. The sets of time series data for the parameter tuning and the performance test are defined as

$$D^{\text{tune}} := \{D^{\pm 10}, D^{\pm 20}, D^{\pm 35}, D^{\pm 40}\} \quad (41)$$

and

$$D^{\text{test}} := \{D^{-10}, D^{+20}, D^{-35}, D^{+40}\}, \quad (42)$$

respectively.

4.4. Problem formulation

In this study, the performance of the maneuvering model with the given parameter $\hat{\theta} \in \hat{\Theta}$ was defined based on the comparison of the simulated time series of maneuvering motion and the real-scale ship trial data. Here, the deviation of the simulated time series following Eq. (12) with the MMG model and the time series of real-scale ship trial was computed, and the candidate parameter $\hat{\theta}$ which minimizes this deviation was output as the optimal value in the parameter tuning problem. This minimization problem is summarized as follows.

$$\begin{aligned} & \underset{\hat{\theta} \in \hat{\Theta}}{\text{minimize}} \quad J(\hat{\theta}; D^{\text{tune}}) := \sum_{D \in D^{\text{tune}}} \sum_{i=2}^T \tilde{p}^{i\top} Q \tilde{p}^i \\ & \text{s.t.} \quad \begin{cases} \tilde{p}^i := \hat{p}^i - p^i \\ \hat{p}^i := (\hat{\zeta}_1^i \hat{\zeta}_2^i \hat{\zeta}_3^i)^\top \\ \hat{\zeta}^i = \hat{\zeta}^{i-1} + f_{\zeta}(\hat{\zeta}^{i-1}, \tau^{i-1}; \hat{\theta}) \Delta t \\ \hat{\zeta}^1 = \zeta^1 \end{cases} \quad (43) \\ & \text{for } i = 2, \dots, T \end{aligned}$$

Here $Q \in \mathbb{R}^{3 \times 3}$ is a weight matrix for deviation \tilde{p} .

The solution of the minimization problem Eq. (43) was explored using CMA-ES. This exploration algorithm is detailed in Sec.5. In the following, the output of CMA-ES for the problem Eq. (43) is described as θ^* .

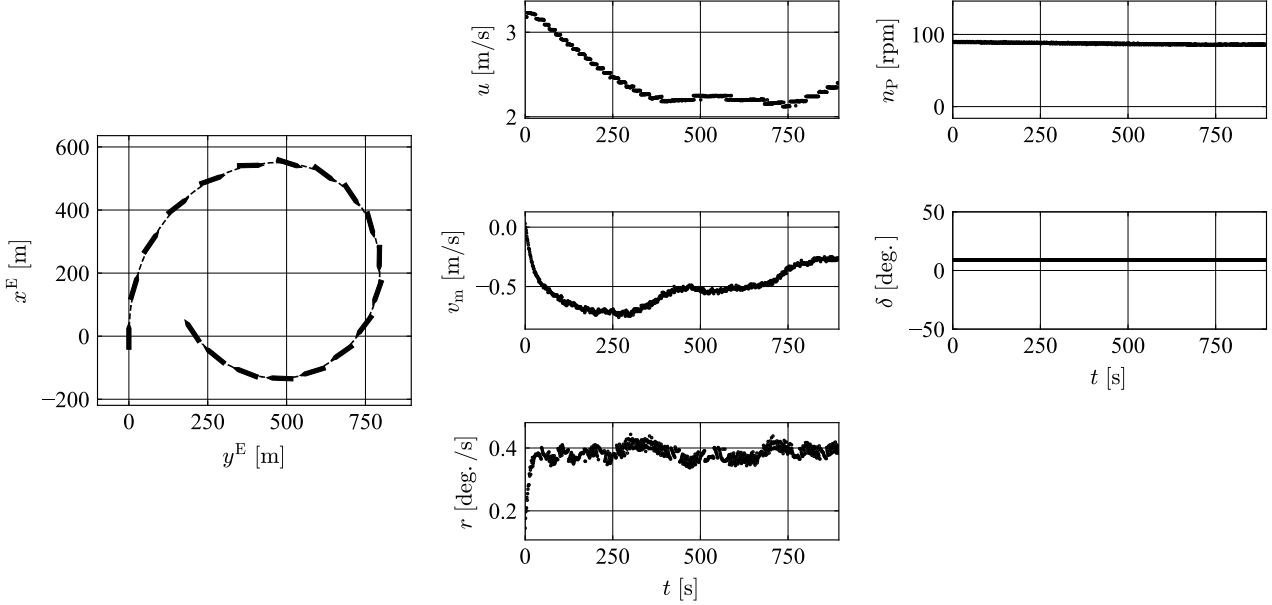


Fig. 2: An example of time series data of real-scale ship trial prepared in this study: turning test with $\delta = 10$ deg..

5. Covariance Matrix Adaption Evolutionary Computation (CMA-ES)

CMA-ES (Hansen, 2007; Hansen and Auger, 2014) is a numerical solver for optimization problems and is known to have high efficiency in the exploration of the optimal solution. In the field of ship navigation, CMA-ES has been applied, for instance, to the optimal control problem for autonomous berthing (Maki et al., 2020) and the parameter exploration problem for the MMG model based on SI (Miyachi et al., 2022a). In general, evolutionary computation does not need the gradient of the objective function. Therefore, users do not have to consider the differentiability of the designed objective function. Although the minimization problem treated in this study includes the computation of maneuvering motion based on the nonlinear and uncontinuous MMG model, the exploration of the optimal solution with CMA-ES is not inappropriate, as the problem is similar to the one in the paper by Miyachi et al. (2022a) where CMA-ES succeeded in the exploration. In the implementation of CMA-ES in this study, the box constraint was handled based on the method proposed by Sakamoto and Akimoto (2017).

The algorithm of CMA-ES is summarized as follows. The values of the objective function for candidate solutions which are generated following the normal distribution defined with a given mean and a given covariance matrix are iteratively calculated. At each step, the algorithm updates the mean and the covariance matrix of the distribution based on the values of the objective function. This iterative update is continued until the convergence of the distribution, and the resultant value of the mean is output as the optimal solution.

In this research, CMA-ES with the restart strategy (Auger and Hansen, 2005) was applied.

6. Results

6.1. Verification of MMG model with pre-determined parameters

For the verification of the MMG model, the simulation of maneuvering motion was conducted with pre-determined parameters shown in Tabs. 3 to 6. This simulation was calculated by applying Euler method to Eq. (12) with time step size: $\Delta t = 1.0$ s. The initial state was $p(0) = (0 \ 0 \ 0)^T$, $u(0) = 6$ knots = 3.086 m/s, $v_m(0) = r(0) = 0$. The control input was fixed as $n_p = 106$ rpm, $\delta = \pm 35$ deg.. These conditions were equivalent to the ones set in the simulation shown in Fig.17 (Section 5.3.1) in the original paper (Okuda et al., 2023). The simulated time series is shown in Fig. 3. Fig. 3 shows that the simulated turning motion matches the one shown in the original paper (Okuda et al., 2023) in that the diameter of the right turning circle is larger than that of the left turning circle. This result verifies the MMG model set in this study.

6.2. Parameter tuning

The weight matrix was set as $Q = \text{diag}(L_{pp}, L_{pp}, 0.25\pi)$. The initial population size was set $\lambda = 12$, and the population size was doubled at the restart of exploration with the upper limit $\lambda \leq \bar{\lambda} = 128$.

First, the process of the exploration by CMA-ES is explained. The case of exploration with $a_r = 0.2$ is shown in Fig. 4. The horizontal axis of Fig. 4 shows the number of iterations, The vertical axis of the upper figure of Fig. 4 shows the smallest value of the objective function calculated

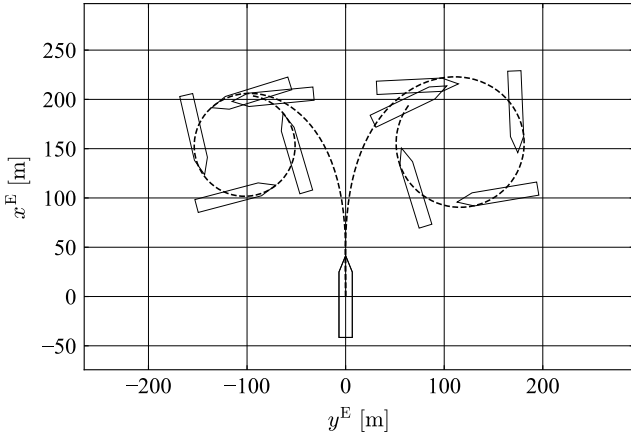


Fig. 3: The trajectory of turning motion simulated based on the MMG model with pre-determined values ($\delta = \pm 35$ deg.).

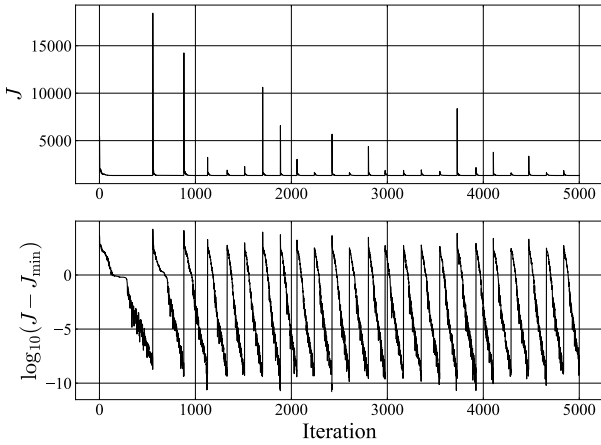


Fig. 4: Exploring process of CMA-ES ($a_r = 0.2$).

for each of the candidate solutions at the iteration. The vertical axis of the lower figure of Fig. 4 shows the value plotted in the upper figure minus the smallest value of the objective function recorded in all iterations. The iteration at which the value of J increases abruptly represents the timing when the convergence of the distribution is confirmed and the exploration restarts with randomly initialized candidate solutions. From Fig. 4, it can be confirmed that the value of J has repeatedly converged to the same value. Not only in the case of $a_r = 0.2$, but also in all the cases conducted in this study, it was confirmed that the optimal solution was explored with a process similar to Fig. 4. Since multiple restarts were observed in a single trial of the algorithm, and convergence to the same value was observed at each restart, the exploration algorithm for each case was run only once in this study.

Second, the performance of the tuned parameter is shown. For each θ^* explored in each a_r , the values of the objective function $J(\cdot)$ were computed for the data set $\mathcal{D}^{\text{tune}}$ and $\mathcal{D}^{\text{test}}$. These values are shown in Figs. 5 and 6. It can be confirmed that the value of $J(\theta^*; \mathcal{D}^{\text{tune}})$ decreases

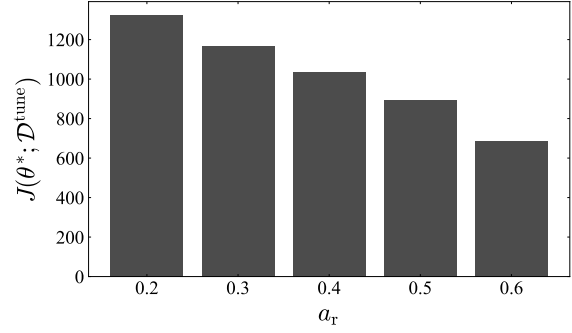


Fig. 5: Values of the objective function on the tuned parameter for tuning data $\mathcal{D}^{\text{tune}}$.

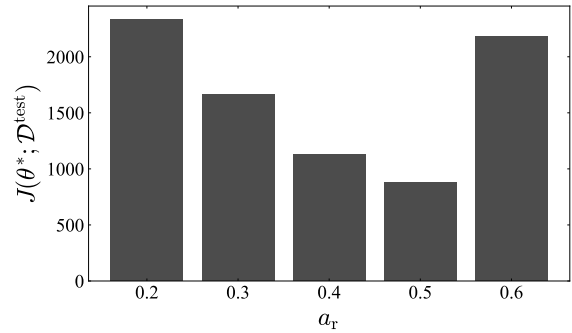


Fig. 6: Values of the objective function on the tuned parameter for test data $\mathcal{D}^{\text{test}}$.

as the value of a_r increases. This means that the accuracy of the simulated maneuvering motion for the tuning data was improved by expanding the exploration range of the target parameter. The value of $J(\theta^*; \mathcal{D}^{\text{test}})$ has the minimum and the maximum at $a_r = 0.5$ and $a_r = 0.6$, respectively. In the range from $a_r = 0.2$ to $a_r = 0.5$, the wider the exploration range, the more accurate the MMG model with the tuned parameter applied. However, in the case $a_r = 0.6$, while showing the best accuracy for tuning data, the value of $J(\theta^*; \mathcal{D}^{\text{test}})$ is larger than the other cases. In the case $a_r = 0.6$, it is considered that the exploration of the parameter that can simulate the maneuvering motion more consistent with the tuning data was performed by expanding the exploration range, resulting in overfitting biased toward the tuning data.

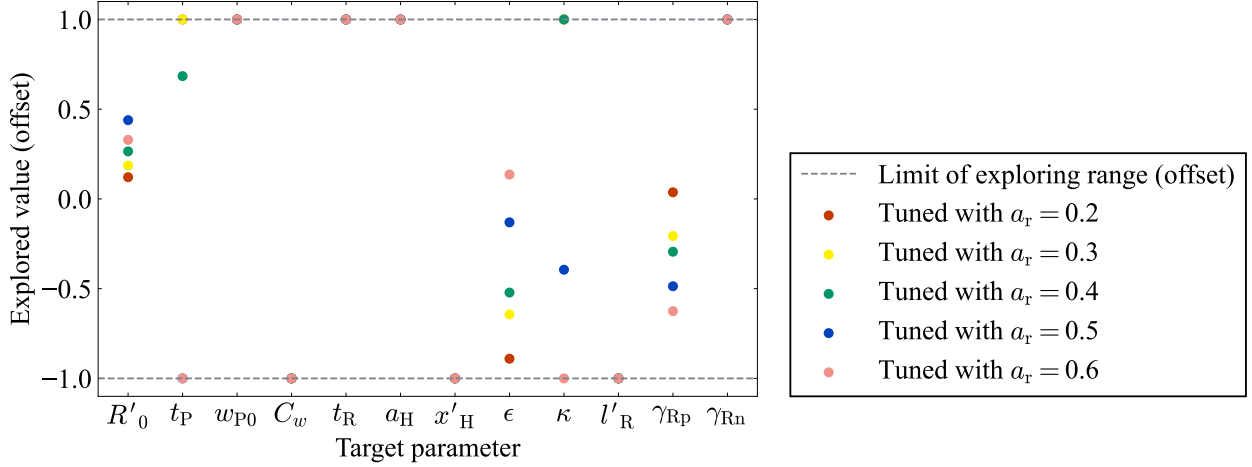
The output values of the target parameters in the exploration with $a_r = 0.2 \sim 0.6$ are shown in Tab. 7. In addition, the distribution of each element of the output parameter in its exploration range is shown in Fig. 7. In Fig. 7, the exploration range $\hat{\Theta}_i$ is offset to $[-1, 1]$, and the values of each parameter are also offset. From Fig. 7, it is observed that, in all cases, w_{p0} , C_w , t_R , a_H , l'_R and γ_{Rn} converged to boundary values on the same side of the exploration range, respectively.

Finally, the time series data of the four real-scale ship trials included in $\mathcal{D}^{\text{test}}$ were compared with the time series simulated based on the MMG model with the pre-determined and tuned parameter. The comparisons are shown in Figs. 8

Table 7

Explored values of target parameters.

a_r	R'_0	t_P	w_{P0}	C_w	t_R	a_H	x'_H	ϵ	κ	l'_R	γ_{Rp}	γ_{Rn}
0.2	0.0174	0.0960	0.5064	-2.4000	-0.0464	0.1896	-0.7260	1.0438	0.6000	-1.0656	0.4866	0.2064
0.3	0.0179	0.1040	0.5486	-2.6000	-0.0406	0.2054	-0.7865	1.0248	0.6500	-1.1544	0.4531	0.2236
0.4	0.0188	0.1019	0.5908	-2.8000	-0.0348	0.2212	-0.8470	1.0049	0.7000	-1.2432	0.4262	0.2408
0.5	0.0207	0.0400	0.6330	-3.0000	-0.0290	0.2370	-0.9075	1.1872	0.4014	-1.3320	0.3655	0.2580
0.6	0.0204	0.0320	0.6752	-3.2000	-0.0232	0.2528	-0.9680	1.3736	0.2000	-1.4208	0.3017	0.2752


Fig. 7: Distribution of the explored values of target parameters in their exploration ranges.

to 11, respectively. All of the real-scale ship trials shown in Figs. 8 to 11 were not used in the parameter tuning phase. By comparing these with the simulated time series using the MMG model with the tuned parameters, the estimation performance of the tuned parameter on the real-scale ship maneuvering motion can be evaluated. From trajectories in the left figure of each of Figs. 8 to 11, in all cases of $a_r = 0.2 \sim 0.6$, the MMG models with the tuned parameter simulate time series closer to the maneuvering motion of the real-scale ship than the one with the pre-determined values. Comparing the best-performing case $a_r = 0.5$ (blue-colored) and the worst-performing case $a_r = 0.6$ (coral pink-colored), although the turning circle diameter differs by about $1.5L_{pp}$ for D^{-10} , not much difference in simulated maneuvering motion is observed for D^{+20} , D^{-35} , and D^{+40} .

7. Discussion

From Figs. 8 to 11, it is confirmed that the parameters were tuned to simulate the turning motions with larger diameters than pre-determined parameters in all cases. Here, Fig. 7 shows that $a_H > 0$ is tuned to be large and $x'_H < 0$ is tuned to be small in all cases, suggesting that N_R is computed to be large. On the other hand, w_{P0} and t_R were tuned to be large so that the propeller inflow velocity u_p and the fraction of rudder $(1 - t_R)F_N \sin \delta$ are computed to be small, respectively. It is analyzed that these effects are

dominant compared to the effect of largely estimated rudder moment N_R .

Among the parameter tunings conducted in this study, the parameter with the best performance on the test data was obtained with the exploration range defined by $a_r = 0.5$. However, the proposed tuning method depends on the time series data set of the real-scale ship trial used for fine-tuning. When tuning the parameters of a maneuvering model, unexpected problems such as overfitting may occur depending on the time series data used for tuning, the target parameters to be tuned, and the exploration range of each parameter, as observed in Fig. 6. Therefore, for parameters explored under different conditions, it is not possible to determine which output is the best for the simulation of the real-scale ship maneuvering motion without at least checking the accuracy of simulated maneuvering motion for time series data other than D^{tune} , such as D^{test} in this study. Thus, if there is a sufficient amount of time series data available for parameter tuning, it is desirable to prepare test data separately from the tuning data and compare the performance against validation data to determine the best parameter.

However, the amount of available time series data of real-scale ship maneuvering motion is limited. Therefore, there may be cases where it is not possible to prepare validation data. In such cases, parameters tuned in a certain condition would have to be used in practice without performance validation. In this case, one should be careful

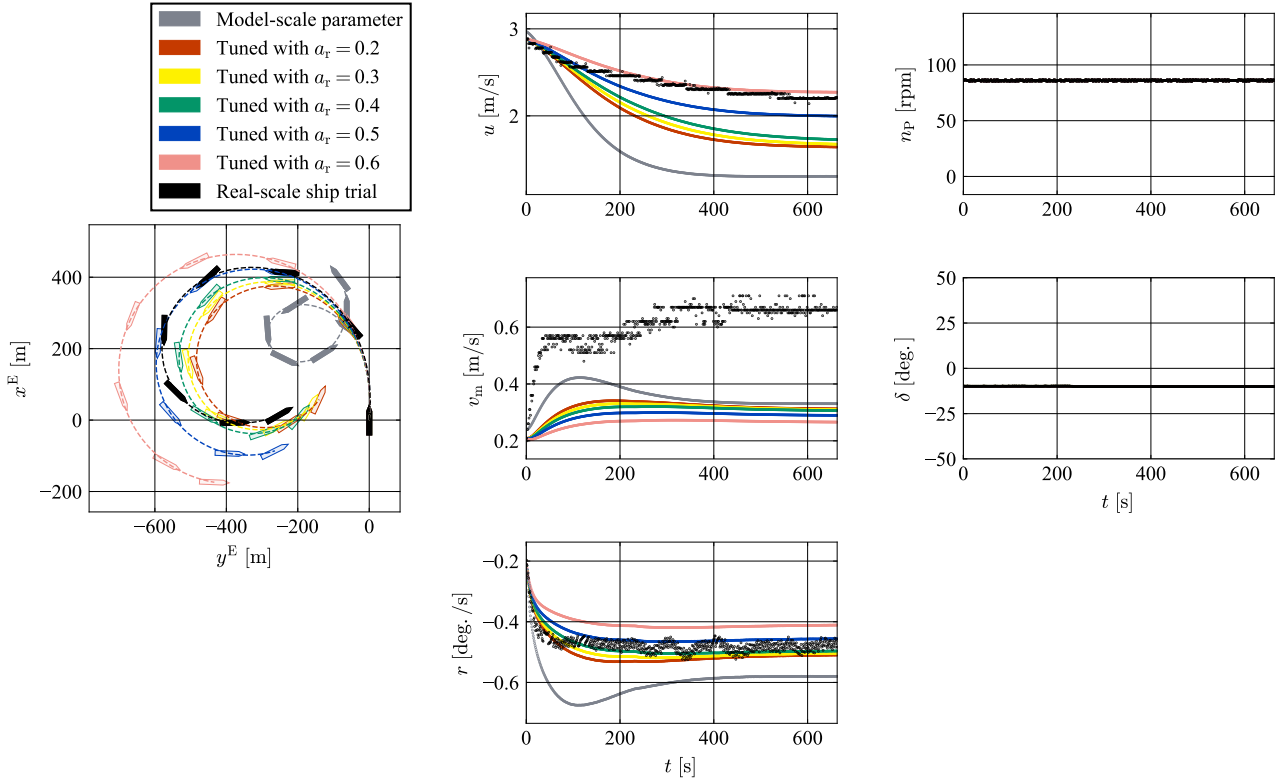


Fig. 8: Comparison of seven time series data of turning test ($\delta = -10$ deg.) which is not utilized in parameter tuning: real-scale ship trial D^{-10} , simulation by the MMG model with untuned parameters, and simulation by the MMG model with tuned parameters ($a_r = 0.2 \sim 0.6$).

not to set an unnecessarily wide exploration range, since parameters may be explored biased toward the tuning data.

8. Concluding remarks

An automatic fine-tuning method for all of the arbitrarily indicated target parameters of the MMG model was proposed. The proposed method tunes the parameter values which are previously determined based on the hydrodynamics, captive model tests, and CFD to the ones for the MMG model of the real-scale ship using the framework of SI. The previously determined parameter values are utilized to constrain the tuned parameter values to the realistic ranges. By directly referring to the time series data of real-scale ship maneuvering motion, the proposed method can steadily improve the performance of the MMG model with the tuned parameter in terms of the accuracy of the simulated maneuvering motion. The proposed fine-tuning method was applied to a container ship and validated with 12 target parameters which is highly influential in the MMG model. In all cases of parameter fine-tuning conducted with different widths of exploration range, better parameters were obtained compared to untuned parameters in terms of the accuracy of the simulated real-scale trajectories.

CRedit authorship contribution statement

Rin Suyama: Conceptualization, Formal analysis, Methodology, Software, Visualization, Writing - Original Draft . **Rintaro Matsushita:** Data Curation, Project administration, Writing - Review & Editing . **Ryo Kakuta:** Data Curation, Project administration, Writing - Review & Editing . **Kouki Wakita:** Methodology, Writing - Review & Editing . **Atsuo Maki:** Funding acquisition, Project administration, Supervision, Writing - Review & Editing .

Acknowledgment

This study was conducted as a part of the Nippon Foundation to Support Fully Autonomous Ship Development Project “MEGURI2040”. The authors are thankful to Mr. Takuya Taniguchi (Osaka University) for a helpful discussion. Moreover, this study was supported by a Grant-in-Aid for Scientific Research from the Japan Society for Promotion of Science (JSPS KAKENHI Grant #22H01701) and by the Fundamental Research Developing Association for Shipbuilding and Offshore (REDAS23-5(18A)).

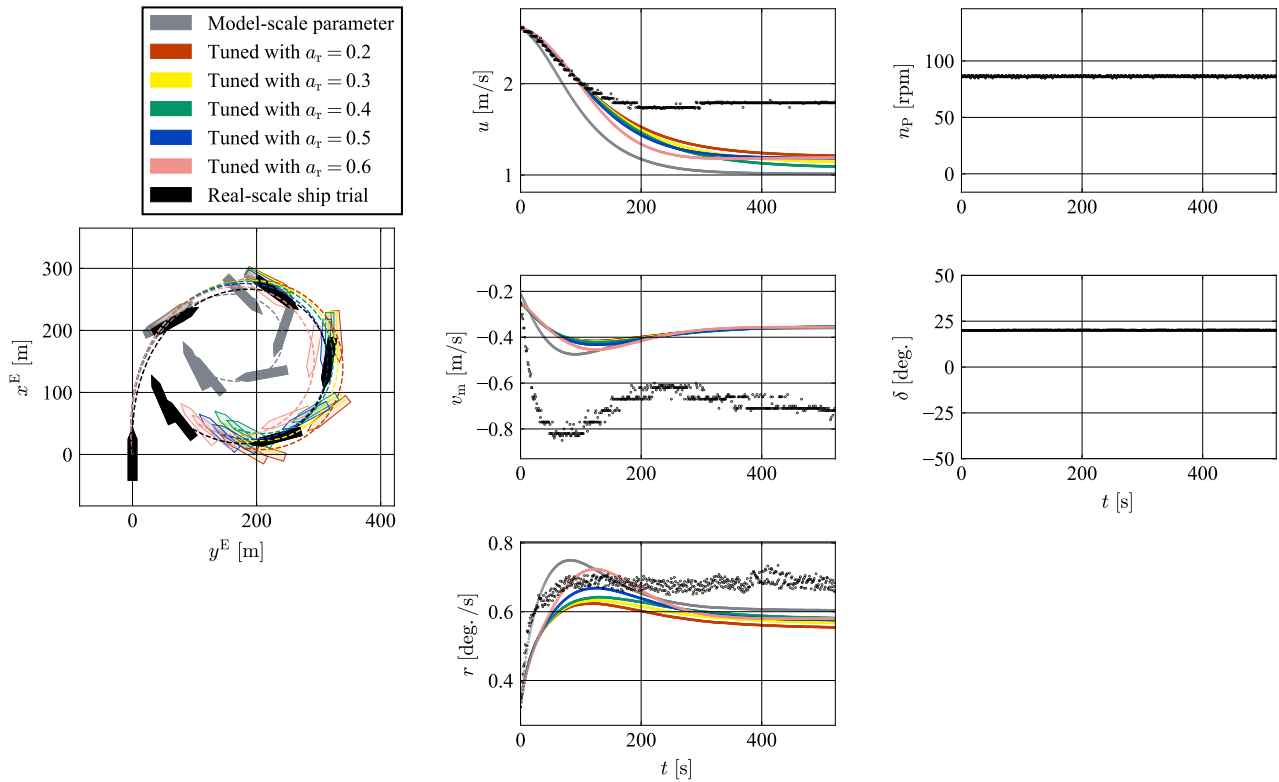


Fig. 9: Comparison of seven time series data of turning test ($\delta = +20$ deg.) which is not utilized in parameter tuning: real-scale ship trial D^{+20} , simulation by the MMG model with untuned parameters, and simulation by the MMG model with tuned parameters ($a_r = 0.2 \sim 0.6$).

References

- Abkowitz, M.A., 1964. Ship hydrodynamics - steering and manoeuvrability. Technical Report. Hydro- and Aerodynamics Laboratory. URL: <https://repository.tudelft.nl/islandora/object/uuid:d511bd6b-ca2e-4f10-ad9f-6c881eb1e9f8?collection=research>.
- Abkowitz, M.A., 1980. Measurement of hydrodynamic characteristics from ship maneuvering trials by system identification. Transactions of Society of Naval Architects and Marine Engineers 88, 283–318. URL: <https://trid.trb.org/view/157366>.
- Aoki, I., Kijima, K., Furukawa, Y., Nakiri, Y., 2006. On the prediction method for maneuverability of a full scale ship. Journal of the Japan Society of Naval Architects and Ocean Engineers 3, 157–165. doi:10.2534/JJASNAOE.3.157. (in Japanese).
- Araki, M., Sadat-Hosseini, H., Sanada, Y., Tanimoto, K., Umeda, N., Stern, F., 2012. Estimating maneuvering coefficients using system identification methods with experimental, system-based, and cfd free-running trial data. Ocean Engineering 51, 63–84. doi:10.1016/j.oceaneng.2012.05.001.
- Auger, A., Hansen, N., 2005. A restart cma evolution strategy with increasing population size, in: 2005 IEEE Congress on Evolutionary Computation, IEEE. pp. 1769–1776. doi:10.1109/CEC.2005.1554902.
- Davidson, K.S., Schiff, L., 1946. Turning and course keeping qualities of ships. Transactions SNAME.
- Dong, Q., Wang, N., Song, J., Hao, L., Liu, S., Han, B., Qu, K., 2023. Math-data integrated prediction model for ship maneuvering motion. Ocean Engineering 285, 115255. doi:10.1016/J.OCEANENG.2023.115255.
- Fossen, T.I., 2011. Handbook of Marine Craft Hydrodynamics and Motion Control. John Wiley and Sons. doi:10.1002/9781119994138.
- Hansen, N., 2007. The CMA Evolution Strategy: A Comparing Review, in: Towards a New Evolutionary Computation. Springer Berlin Heidelberg, pp. 75–102. doi:10.1007/3-540-32494-1_4.
- Hansen, N., Auger, A., 2014. Principled design of continuous stochastic search: From theory to practice, in: Principles of System Identification. Springer, pp. 145–180. doi:10.1007/978-3-642-33206-7_8.
- He, H.W., Wang, Z.H., Zou, Z.J., Liu, Y., 2022. Nonparametric modeling of ship maneuvering motion based on self-designed fully connected neural network. Ocean Engineering 251, 111113. doi:10.1016/J.OCEANENG.2022.111113.
- Inoue, S., Hirano, M., Kijima, K., 1981. Hydrodynamic derivatives on ship manoeuvring. International Shipbuilding Progress 28, 112–125. doi:10.3233/ISP-1981-2832103.
- Kambara, T., Miyauchi, Y., Hosogaya, K., Maki, A., 2022. Fundamental study on estimation of system model for berthing and unberthing of full scale ship, in: Conference proceedings, the Japan Society of Naval Architects and Ocean Engineers, pp. 2022A–OS1–5. URL: https://www.jstage.jst.go.jp/article/conf/35/0/35_29/_article/-char/en. (in Japanese).
- Kim, D., 2018. Estimation of hydrodynamic coefficients from results of real ship sea trials. Polish Maritime Research 25, 65–72. doi:10.2478/pomr-2018-0133.
- Li, R., Li, T., Bu, R., Zheng, Q., Chen, C.L., 2013. Active disturbance rejection with sliding mode control based course and path following for underactuated ships. Mathematical Problems in Engineering 2013. doi:10.1155/2013/743716.
- Luo, W., Zhang, Z., 2016. Modeling of ship maneuvering motion using neural networks. Journal of Marine Science and Application 15, 426–432. doi:10.1007/S11804-016-1380-8/METRICS.

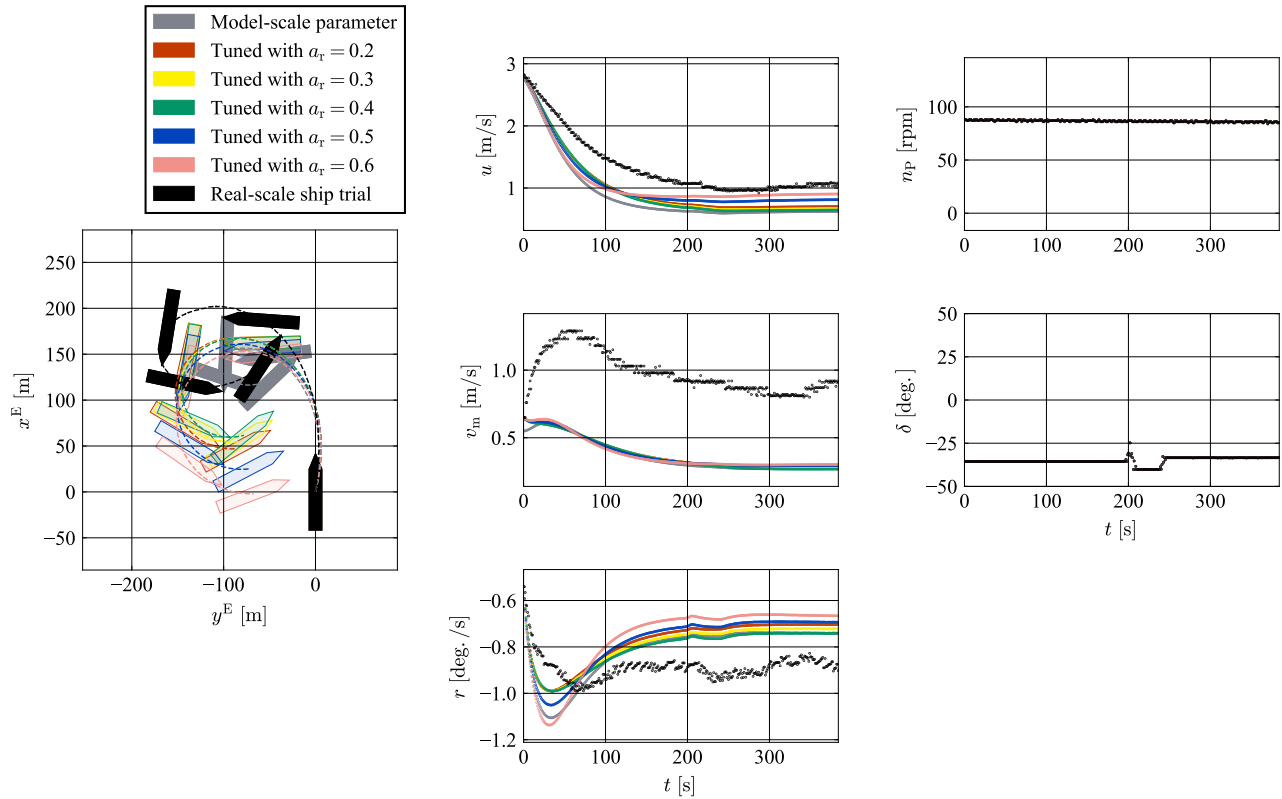


Fig. 10: Comparison of seven time series data of turning test ($\delta = -35$ deg.) which is not utilized in parameter tuning: real-scale ship trial D^{-35} , simulation by the MMG model with untuned parameters, and simulation by the MMG model with tuned parameters ($a_r = 0.2 \sim 0.6$).

- Luo, W.L., Zou, Z., 2009. Parametric identification of ship maneuvering models by using support vector machines. *Journal of Ship Research* 53, 19–30. URL: <https://onepetro.org/JSR/article-abstract/53/01/19/175116/Parametric-Identification-of-Ship-Maneuvering?redirectedFrom=fulltext>.
- Maki, A., Sakamoto, N., Akimoto, Y., Nishikawa, H., Umeda, N., 2020. Application of optimal control theory based on the evolution strategy (cma-es) to automatic berthing. *Journal of Marine Science and Technology* 25, 221–233. doi:10.1007/s00773-019-00642-3.
- Meng, Y., Zhang, X., Zhu, J., 2022. Parameter identification of ship motion mathematical model based on full-scale trial data. *International Journal of Naval Architecture and Ocean Engineering* 14, 100437. doi:10.1016/j.ijnaoe.2022.100437.
- Miyauchi, Y., Akimoto, Y., Umeda, N., Maki, A., 2023. Development of a mathematical model for harbor-maneuvers to realize modeling automation. *arXiv:2302.10459*.
- Miyauchi, Y., Maki, A., Umeda, N., Rachman, D.M., Akimoto, Y., 2022a. System parameter exploration of ship maneuvering model for automatic docking / berthing using cma-es. *Journal of Marine Science and Technology* 27, 1065–1083.
- Miyauchi, Y., Sawada, R., Akimoto, Y., Umeda, N., Maki, A., 2022b. Optimization on planning of trajectory and control of autonomous berthing and unberthing for the realistic port geometry. *Ocean Engineering* 245, 110390. doi:10.1016/j.oceaneng.2021.110390.
- Moreira, L., Soares, C.G., 2003. Dynamic model of manoeuvrability using recursive neural networks. *Ocean Engineering* 30, 1669–1697. doi:10.1016/S0029-8018(02)00147-6.
- Motora, S., 1955. Course stability of ships. *Journal of Zosen Kiokai* 77, 69–90. URL: https://www.jstage.jst.go.jp/article/jjasnaoe1903/1955/77/1955_77_69/_pdf. (in Japanese).
- Motora, S., 1959. On the measurement of added mass and added moment of inertia for ship motions. *Journal of Zosen Kiokai* 1959, 83–92. doi:10.2534/jjasnaoe1952.1959.83.
- Nomoto, K., Taguchi, T., Honda, K., Hirano, S., 1957. On the steering qualities of ships. *International Shipbuilding Progress* 4, 354–370.
- Ogawa, A., Kasai, H., 1978. On the mathematical model of manoeuvring motion of ships. *International Shipbuilding Progress* 25, 306–319. doi:10.3233/ISP-1978-2529202.
- Okuda, R., Yasukawa, H., Yamashita, T., Matsuda, A., 2023. Maneuvering simulations at large drift angles of a ship with a flapped rudder. *Applied Ocean Research* 135, 103567. doi:10.1016/J.APOR.2023.103567.
- Oskin, D.A., Dyda, A.A., Markin, V.E., 2013. Neural network identification of marine ship dynamics. *IFAC Proceedings Volumes* 46, 191–196. doi:10.3182/20130918-4-JP-3022.00018.
- Rajesh, G., Bhattacharyya, S.K., 2008. System identification for nonlinear maneuvering of large tankers using artificial neural network. *Applied Ocean Research* 30, 256–263. doi:10.1016/J.APOR.2008.10.003.
- Ramirez, W.A., Leong, Z.Q., Nguyen, H., Jayasinghe, S.G., 2018. Non-parametric dynamic system identification of ships using multi-output gaussian processes. *Ocean Engineering* 166, 26–36. doi:10.1016/J.OCEANENG.2018.07.056.
- Sakamoto, N., Akimoto, Y., 2017. Modified box constraint handling for the covariance matrix adaptation evolution strategy, in: *Genetic and evolutionary computation conference, Association for Computing Machinery (ACM)*. pp. 183–184. doi:10.1145/3067695.3075986.
- Sakamoto, N., Ohashi, K., Araki, M., Ichi Kume, K., Kobayashi, H., 2019. Identification of kvlcc2 manoeuvring parameters for a modular-type mathematical model by rans method with an overset approach. *Ocean*

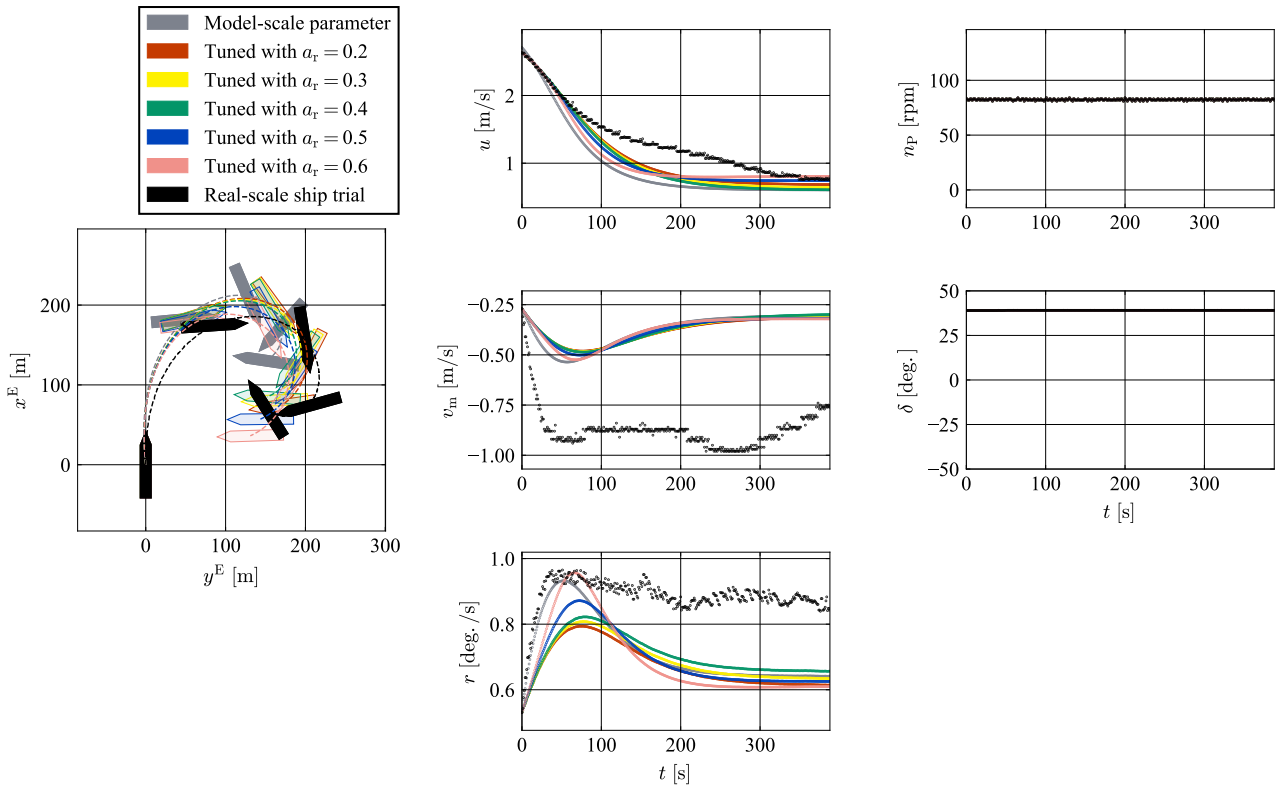


Fig. 11: Comparison of seven time series data of turning test ($\delta = +40$ deg.) which is not utilized in parameter tuning: real-scale ship trial D^{+40} , simulation by the MMG model with untuned parameters, and simulation by the MMG model with tuned parameters ($a_r = 0.2 \sim 0.6$).

- Engineering 188, 106257. doi:10.1016/J.OCEANENG.2019.106257.
- Sutulo, S., Soares, C.G., 2014. An algorithm for offline identification of ship manoeuvring mathematical models from free-running tests. *Ocean Engineering* 79, 10–25. doi:10.1016/j.oceaneng.2014.01.007.
- Sutulo, S., Soares, C.G., 2023. Application of an offline identification algorithm for adjusting parameters of a modular manoeuvring mathematical model. *Ocean Engineering* 279, 114328. doi:10.1016/J.OCEANENG.2023.114328.
- Suyama, R., Miyauchi, Y., Maki, A., 2022. Ship trajectory planning method for reproducing human operation at ports. *Ocean Engineering* 266, 112763. URL: <https://doi.org/10.1016/j.oceaneng.2022.112763>.
- Wakita, K., Maki, A., Umeda, N., Miyauchi, Y., Shimoji, T., Rachman, D.M., Akimoto, Y., 2022. On neural network identification for low-speed ship maneuvering model. *Journal of Marine Science and Technology* 27, 772–785. doi:10.1007/s00773-021-00867-1.
- Wang, Z., Kim, J., Im, N., 2023. Non-parameterized ship maneuvering model of deep neural networks based on real voyage data-driven. *Ocean Engineering* 284, 115162. doi:10.1016/J.OCEANENG.2023.115162.
- Wang, Z., Xu, H., Xia, L., Zou, Z., Soares, C.G., 2020. Kernel-based support vector regression for nonparametric modeling of ship maneuvering motion. *Ocean Engineering* 216, 107994. doi:10.1016/J.OCEANENG.2020.107994.
- Woo, J., Park, J., Yu, C., Kim, N., 2018. Dynamic model identification of unmanned surface vehicles using deep learning network. *Applied Ocean Research* 78, 123–133. doi:10.1016/J.APOR.2018.06.011.
- Xue, Y., Liu, Y., Ji, C., Xue, G., Huang, S., 2020. System identification of ship dynamic model based on gaussian process regression with input noise. *Ocean Engineering* 216, 107862. doi:10.1016/J.OCEANENG.2020.107862.
- Yasukawa, H., Yoshimura, Y., 2015. Introduction of mmg standard method for ship maneuvering predictions. *J Mar Sci Technol* 20, 37–52. doi:10.1007/s00773-014-0293-y.
- Yoon, H.K., Rhee, K.P., 2003. Identification of hydrodynamic coefficients in ship maneuvering equations of motion by estimation-before-modeling technique. *Ocean Engineering* 30, 2379–2404. doi:10.1016/S0029-8018(03)00106-9.
- Zhang, C., Liu, X., Wan, D., Wang, J., 2019. Experimental and numerical investigations of advancing speed effects on hydrodynamic derivatives in mmg model, part i: X_{vv}, y_{vv}, n_v . *Ocean Engineering* 179, 67–75. doi:10.1016/j.oceaneng.2019.03.019.
- Zhang, Q., ku Zhang, X., kyun Im, N., 2017. Ship nonlinear-feedback course keeping algorithm based on mmg model driven by bipolar sigmoid function for berthing. *International Journal of Naval Architecture and Ocean Engineering* 9, 525–536. doi:10.1016/J.IJNAOE.2017.01.004.
- Zhang, X.G., Zou, Z.J., 2013. Black-box modeling of ship manoeuvring motion based on feed-forward neural network with chebyshev orthogonal basis function. *Journal of Marine Science and Technology* 18, 42–49. doi:10.1007/S00773-012-0190-1/FIGURES/5.
- Zheng, Y., Tao, J., Sun, Q., Sun, H., Chen, Z., Sun, M., Xie, G., 2022. Soft actor-critic based active disturbance rejection path following control for unmanned surface vessel under wind and wave disturbances. *Ocean Engineering* 247, 110631. doi:10.1016/J.OCEANENG.2022.110631.
- Åström, K.J., Källström, C.G., 1976. Identification of ship steering dynamics. *Automatica* 12, 9–22. doi:10.1016/0005-1098(76)90064-9.